

Electronic structure of multiwall boron nitride nanotubesG. G. Fuentes,^{1,*} Ewa Borowiak-Palen,^{1,2} T. Pichler,^{1,3} X. Liu,¹ A. Graff,¹ G. Behr,¹ R. J. Kalenczuk,² M. Knupfer,¹ and J. Fink¹¹Leibniz Institute for Solid State and Materials Research Dresden, P.O. Box 270016, D-01171 Dresden, Germany²Technical University of Szczecin, Institute of Chemical and Environment Engineering, Szczecin, Poland³Universität Wien, Institut für Materialphysik, Strudlhofgasse 4, A-1090 Wien, Austria

(Received 3 September 2002; published 31 January 2003)

We report on electron energy-loss spectroscopy studies of the electronic properties of multiwall boron nitride nanotubes, in terms of the $B1s$ and $N1s$ excitation edges and of the q -dependent energy-loss function. The q -dependent dielectric function shows a strong dispersion in momentum of the π and $\sigma + \pi$ plasmons indicating that they are spatially delocalized along the tube axis as expected according to their characteristic two-dimensional graphiticlike structure, and nondispersing excitations at 11 and 12 eV. The dielectric function ϵ of the boron nitride nanotubes reveals an intense π - π^* interband transition at 5.4 eV, which is shifted to lower energies by 0.6 eV when compared to hexagonal BN in good agreement with recent theoretical band-structure calculations of boron nitride nanotubes.

DOI: 10.1103/PhysRevB.67.035429

PACS number(s): 73.22.-f, 78.67.Ch, 78.20.Ci

I. INTRODUCTION

Since Ijima¹ discovered carbon nanotubes in 1991, the understanding of the unique physical properties of wrapped graphenelike materials²⁻⁴ and their metal filled derivatives^{5,6} have attracted large attention among researchers. The existence of the equivalent metastable allotropic form of hexagonal boron nitride (h -BN) was recently proposed using tight-binding calculations by Rubio *et al.*⁷ on the basis of the similarities between lattice structure and bonding length of graphite and h -BN. The band structure for this new class of metastable structures was predicted to have a large band gap leading to promising potential uses in blue and violet photoluminescence devices.⁸

During the last years BN nanotubes have been fabricated using different methods. Loiseau *et al.*⁹ synthesized bundles of hexagonal-like multiwall BN nanotubes using arc discharge of HfB_2 electrodes in nitrogen atmosphere. Han *et al.*¹⁰ proposed a route based on the chemical substitution of carbon by B and N from a template of single wall carbon nanotubes (SWCNT's) using B_2O_3 powders as boron source in a N_2 atmosphere. Under the same conditions, Golberg *et al.*^{11,12} found a sharp enhancement of the production yield of multiwall BN nanotubes by adding MoO_3 as catalyst. More recently, Zhi *et al.*¹³ characterized the photoluminescence of aligned multiwall BN nanotubes synthesized by chemical vapor deposition (CVD) and pulsed-arc discharge. Theoretical band-structure and lattice energy calculations of BN nanotubes have also been reported in the literature.^{7,14-17} Simple tight-binding calculations⁷ predict a direct band gap for zigzag ($n,0$) BN nanotubes and an indirect gap for armchair (n,n) nanotubes in contrast to SWCNT's where the chirality defines the metallic or the semiconducting character of the tube. The same band-structure calculations^{7,14} showed that BN nanotubes have a band-gap dependence on the diameter of the tube which is stronger in the case of zigzag tubes. Moreover, it was also predicted that the band gap of large diameter BN nanotubes shows only little dependence on the chirality.^{7,14} Minimal lattice energy calculations sug-

gest that the most favorable chirality for BN nanotubes is zigzag, although electron-diffraction measurements of multiwall BN nanotubes¹¹⁻¹³ evidence the presence of armchair chirality in a proportion larger than 15%. Hernández *et al.*¹⁸ also predicted a Young Modulus of around 300 GPa for both zigzag and armchair nanotubes and some degree of buckling perpendicular to the nanotube axis that increases as the inner radius of the nanotube decreases. Furthermore, Kim *et al.*¹⁷ theoretically predicted a band-gap reduction in BN nanotubes by applying an external pressure perpendicular to the tube axis, as due to the decrease of the effective radius of the tube, which would also lead to interesting applications. Finally, Okada *et al.*¹⁹ reported on the band structure of C_{60} encapsulated into BN nanotubes. Non-momentum-resolved EELS studies on multiwall BN nanotubes have been reported by Terauchi *et al.*²⁰ and Loiseau *et al.*⁹ Nevertheless, experimental characterisations of the electronic properties of BN nanotubes are still scarce.

In this work we present an electron energy-loss spectroscopy (EELS) study of high purity multiwall BN nanotubes in terms of the $B1s$ and $N1s$ excitation edges and momentum dependent energy-loss functions $\text{Im}\{-1/\epsilon(\omega, q)\}$. The q -dependent dielectric properties and electronic structure of the BN nanotubes are compared with those reported in the literature for bulk h -BN, as well as with recent theoretical and experimental results of single wall and multiwall BN nanotubes.

II. EXPERIMENT

Multiwall BN nanotubes have been grown by following the route proposed by Golberg *et al.*^{11,12} based on the substitution of carbon atoms from pristine SWCNT's by boron and nitrogen. The details of the preparation of the SWCNT's used as template can be found elsewhere.²¹ The reaction was carried out in N_2 atmosphere at 1500 °C for 30 min using a mixture of 5:2:1 in weight of B_2O_3 , MoO_3 , and SWCNT, respectively. For the EELS measurements, a KBr crystal was covered drop by drop by a suspension of raw material in

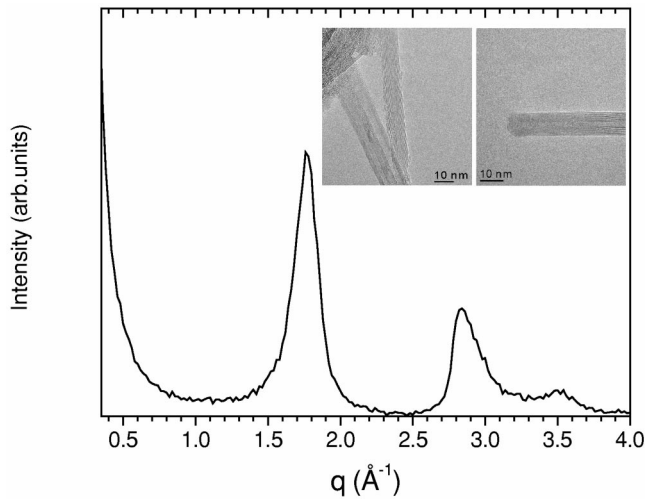


FIG. 1. Electron-diffraction profile of multiwall BN nanotubes after annealing in UHV. The inset shows typical high-resolution TEM pictures of BN nanotubes.

CCl_4 until an effective thickness of about 100 nm was reached. Subsequently, the film was floated off in distilled water and mounted on standard 1000 mesh copper microscopy grids. The samples were heated in UHV up to 450 °C to remove organic contaminations without changing the structure of the nanotubes. The EELS measurements were carried out using a dedicated 170-keV spectrometer described in detail elsewhere.²² The energy and momentum resolution was set to 180 meV and 0.03 \AA^{-1} , respectively, for the electron diffraction and for the low energy-loss function. In the case of the core-level excitations we used an energy and momentum resolution of 330 meV and 0.1 \AA^{-1} , respectively. The loss function $[\text{Im}\{-1/\epsilon(\omega, q)\}]$, which is proportional to the dynamic structure factor $S(\omega, q)$, has been monitored at different momentum transfer q . The probing area of the primary electron beam is about 1 mm^2 , i.e., the information obtained represents an average over a large numbers of nanotubes.

III. RESULTS

A. Electron-diffraction and core-level excitations

Figure 1 shows the electron-diffraction pattern of as-grown BN nanotubes after annealing in vacuum, together with typical high-resolution TEM micrographs (cf. inset of Fig. 1). The TEM image shows the multiwall BN nanotubes with a number of BN layers between 4 and 10. The averaged inner diameter of the nanotubes as measured over several TEM pictures is around 3.1 nm (with a standard deviation of 0.8 nm), which is larger than the diameter of the SWCNT used as templates, and slightly larger than that reported by Loiseau *et al.*⁹ (2.5 nm) and Golberg *et al.*¹² (2.1 nm as estimated from Fig. 1 in Ref. 12).

The chemical analysis of the TEM images using *in situ* EELS indicates that B and N constitute the nanotubular structures in a 1 to 1 atomic ratio. In addition, some TEM pictures also showed traces of *h*-BN aggregated in lamella-

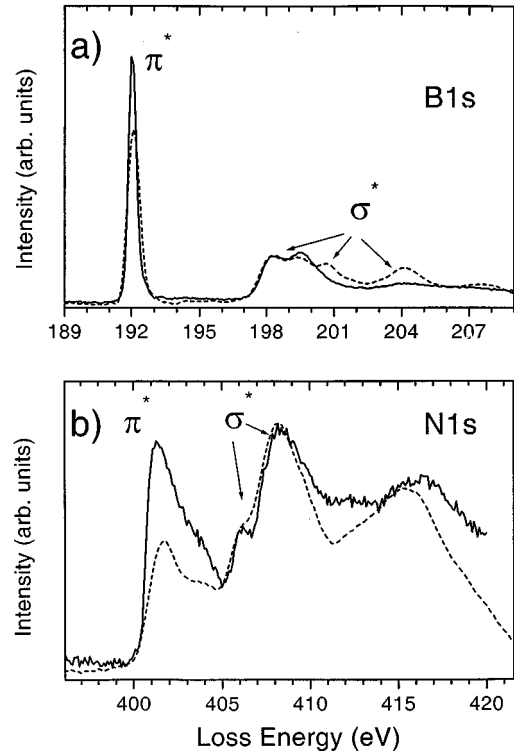


FIG. 2. (a) $B1s$ and (b) $N1s$ excitation spectra of BN nanotubes as measured by EELS (solid). (a) $B1s$ and (b) $N1s$ excitation spectra of polycrystalline *h*-BN (dashed) as measured using synchrotron radiation (taken from Ref. 25).

type structures, and the presence of denser material, likely catalytic particles, filling the end of some of the nanotubes. The electron-diffraction pattern reveals two intense features at 1.7 and 2.8 \AA^{-1} corresponding to a distance between BN sheets of 0.35 nm and an in-plane lattice parameter “ a ” of 0.22 nm, respectively, and a smaller peak at 3.5 \AA^{-1} . As compared to the values referenced in the literature for *h*-BN, the distance between two BN sheets in our nanotubes exhibits a slight expansion of 6%. Loiseau *et al.*⁹ have also reported a similar expansion in multiwall BN nanotubes synthesised by arc discharge. Moreover, the interplanar distance in multiwall carbon nanotubes^{23,24} between their graphitic sheets is enlarged with respect to that found in bulk graphite. In addition, the lattice constant a is slightly smaller than the corresponding value of *h*-BN, though the corresponding displacement in q is smaller than the resolution of the spectrometer.

The core-level electronic structure can be examined by measuring the $B1s$ and $N1s$ excitation edges. Figure 2(a) represents the $B1s$ excitation spectrum of multiwall BN nanotubes measured after annealing in vacuum (solid), and a near-edge x-ray-absorption fine structure (NEXAFS) $B1s$ reference spectrum (dashed) from polycrystalline *h*-BN.²⁵ The $B1s$ spectrum of the multiwall BN nanotubes exhibits a sharp peak at 192 eV due to the excitonic $B1s \rightarrow \pi^*$ transition, which is only allowed for momentum transfers perpendicular to the BN sheets.^{26–28} The $B1s \rightarrow \sigma^*$ shows two peaks at 198.2 and 199.5 eV, and a barely resolved weak

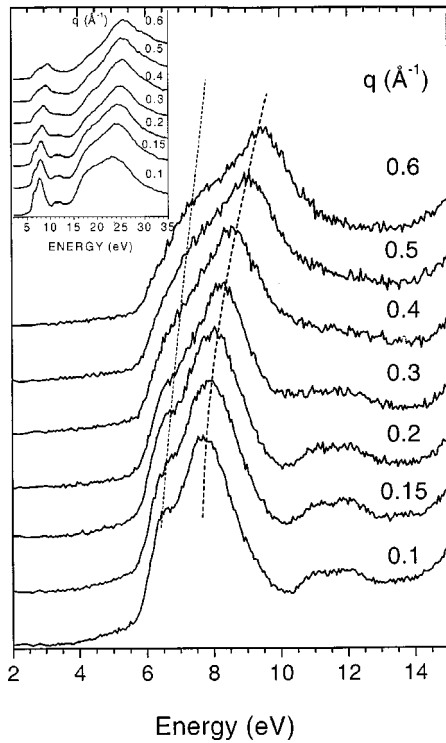


FIG. 3. Loss spectra of the multiwall BN nanotubes between 2 and 15 eV as a function of the momentum transfer q , as measured by EELS. Inset: full energy range between 0 and 30 eV.

feature at 204 eV. The peak at 200.5 eV in the h -BN reference spectrum is clearly absent in the spectrum of our sample. Figure 2(b) represents the N1s excitation spectrum of the multiwall BN nanotubes and the reference N1s NEXAFS spectrum from h -BN.²⁵ The low-energy π^* resonance is observed at 401 eV in good agreement with that detected for h -BN.^{27,28} In addition, the broad σ^* resonance around 408 eV also resembles that observed for h -BN. As in the case of the B1s spectra, the intensity of the π^* resonance relative to the σ^* resonance is larger as compared to the π^*/σ^* ratio for the reference material.

B. Low energy-loss function

The dependence of the energy-loss function upon the momentum transfer q can provide a detailed view on the spatial extension of the electronic excitations, their multipolar character, and their dispersion.^{22,29} The loss spectra of the multiwall BN nanotubes are depicted in Fig. 3 as a function of the momentum transfer q . They are dominated by a strong collective excitation around 23.2 eV involving all π and σ valence electrons and a shoulder at ~ 17 eV associated to the onset of the N2s excitation threshold according to different band-structure calculations.^{26,30} A double-peak feature appears at 6.7 and 7.7 eV in the loss spectra related to π - π^* electronic interband transitions. Both features exhibit a significant dispersion as q increases, as indicated by the dashed lines in Fig. 3. A nondispersive double peak centred at 11 and 12 eV can also be observed for $0.1 < q < 0.3 \text{ \AA}^{-1}$, decreasing

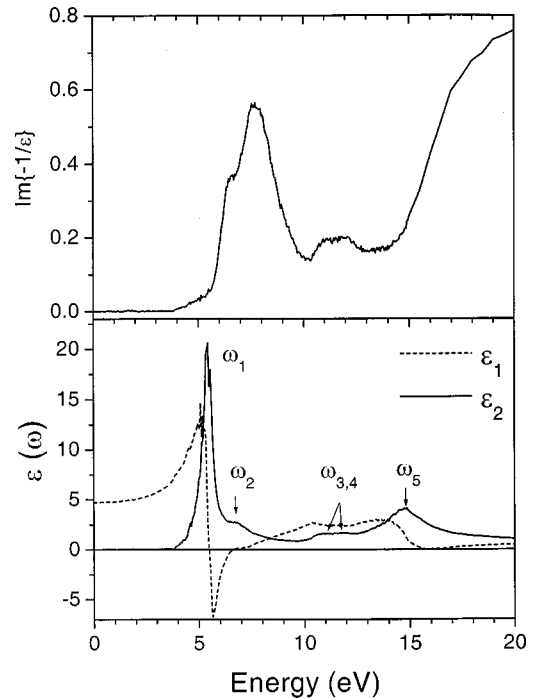


FIG. 4. Loss function and $\varepsilon(\omega, q)$ of multiwall BN nanotubes between $0 < \omega < 20$ eV as derived from the Kramers Kronig analysis for $q = 0.1 \text{ \AA}^{-1}$. Arrows indicate the energy positions of the excitations ω_1 to ω_5 .

in intensity for higher values of q suggesting that they originate from dipole-allowed interband transitions.

The low energy-loss spectra can be better understood in terms of the real and imaginary parts of the dielectric functions, ε_1 and ε_2 , which can be obtained by a Kramers Kronig analysis (KKA) of the measured loss spectra. For the KKA we have determined the effective number of electrons per unit cell contributing to the loss function (N_{eff}) at low q using $\varepsilon_1(0) = 4.7$ from polycrystalline h -BN (Ref. 31), while for higher q values we have maintained N_{eff} , i.e., the sum rule, constant. Following this procedure, $\varepsilon_1(0, q)$ decreases progressively from $\varepsilon_1(0) = 4.7$ in the optical limit down to $\varepsilon_1(0) = 2.2$ for $q = 0.6 \text{ \AA}^{-1}$, which is the expected behavior upon q .³² Figure 4 shows the loss function (upper part), ε_1 (dashed), and ε_2 (solid, bottom part) obtained from the KKA of the loss function at $q = 0.1 \text{ \AA}^{-1}$. ε_2 exhibits an intense excitation at 5.4 eV (ω_1) and a weaker feature at 6.8 eV (ω_2), both corresponding to electronic interband transitions of π character leading to collective excitations at 6.6 and 7.8 eV, as evidenced by the two maxima in the loss function. In addition, ε_2 reveals a double feature centred at 11 eV ($\omega_{3,4}$) which is also reproduced in the loss function and a broad oscillator at 14.7 eV (ω_5), which in bulk h -BN is associated to electronic σ - σ^* (Ref. 30) transitions.

The q dependence of the interband excitations can be examined by comparing the imaginary part of the dielectric function ε_2 for different q . Figure 5 shows $\varepsilon_2(\omega, q)$ for $0.1 < q < 0.6 \text{ \AA}^{-1}$. Furthermore, Fig. 6 displays the energy positions of the electronic excitations (open symbols: $\omega_1 - \omega_5$), and the position of the π and $\sigma + \pi$ plasmon (filled

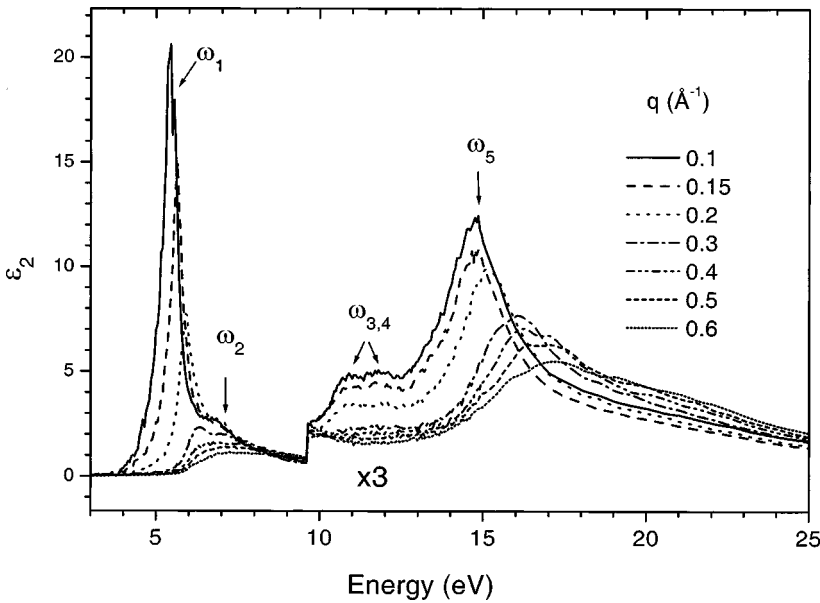


FIG. 5. ϵ_2 of multiwall BN nanotubes between $2 < \omega < 25$ eV as derived from the Kramers Kronig analysis of the loss function of Fig. 3 for different q .

symbols) in the loss function as a function of q . Figure 6 includes the energy positions of the π and $\sigma + \pi$ plasmons as measured by Tarrío *et al.*³³ in pyrolytic h -BN as a function of momentum parallel to the basal planes (dashed lines). It is observed how the lowest energy excitations ω_1 and ω_2 disperse upwards in energy as q increases. In addition, the strength of both excitations decreases sharply as q increases,

as expected for transitions having electric dipolar character. The momentum dispersion of these two excitations leads to the positive dispersion of the π plasmon in the loss function, which is also plotted in Fig. 6. The same behavior upon q is also observed for the π plasmon in h -BN,³³ which confirms the similar electronic nature arising from the hexagonal symmetry of the sheets along the tube axis. The upwards shift of the π plasmon as q increases has been also observed in carbon based materials such as graphite,³⁴ carbon nanotubes,^{35–37} and concentric-shell fullerenes.³⁸

The peaks $\omega_{3,4}$, leading to features in the loss function centred at 11 eV, do not disperse in energy and decrease in strength indicating their dipole allowed character. The equivalent excitation in h -BN appears as one broad peak centred at 11.5 eV. Analogously, the oscillator ω_5 arising from σ - σ^* (Ref. 30) transitions disperses significantly to higher energies as q increases as expected for electronic transitions between broad bands along the tube axis.

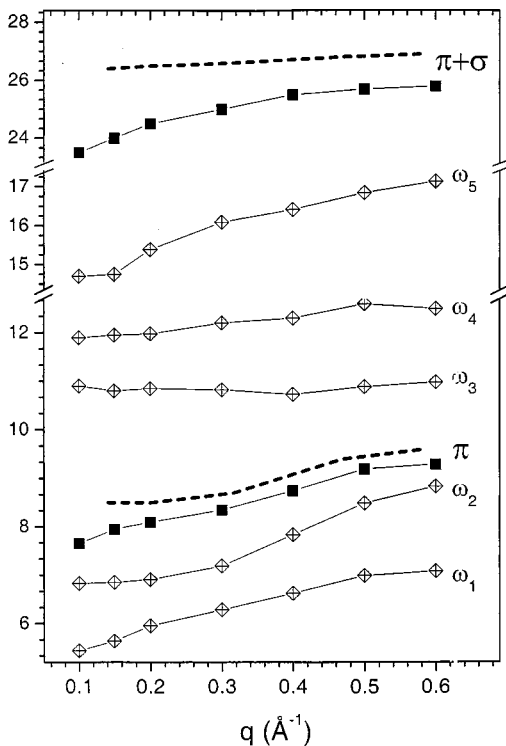


FIG. 6. Energy of the different excitations (open symbols) and plasmons (filled symbols) as a function of q , as derived from Fig. 5. The plasmon energies as derived from Ref. 33 are also included for comparison (dashed lines).

IV. DISCUSSION

Let us consider first the fine structure of the core-level excitations B1s and N1s. The larger intensity of the π^* excitation at 192 eV in the B1s edge [see Fig. 2(a)] and at 401 in the N1s edge [see Fig. 2(b)] relative to that of the σ^* states as compared to the same π^*/σ^* ratio in h -BN is somewhat surprising. In fact, a reduction of the π^*/σ^* ratio is observed in carbon nanotubes with respect to bulk graphite, which is interpreted as due to the appearance of some sp^3 hybridization of the C atoms owing to the curvature of the sheets. A similar enhancement of the π^*/σ^* ratio in the B1s and N1s edges of BN nanotubes was reported by Loiseau *et al.*⁹ We attribute this effect to the fact that the nanotubes are oriented preferentially along the surface plane of the KBr crystal and therefore parallel to the surface of the copper grid, so that, for core-level measurements, where the momentum transfer is chosen perpendicular to the surface of

the copper grid, the contribution of the electronic transitions to final states of π^* character which originate from the $2p_z$ orbitals perpendicular to the BN sheets is enhanced.

The position of the peak ω_1 in the boron nitride nanotubes is downward shifted by 0.6 eV with respect to the value reported for *h*-BN (Refs. 26, 30), which can be explained in terms of the curvature of the BN sheets. As mentioned above, the analysis of the TEM pictures revealed an averaged inner diameter of the tubes of 3.1 ± 0.8 nm. Thus we can estimate the chirality index n for zigzag ($n,0$) or for armchair (n,n) nanotubes by using the equation $d = (a/\pi) \sqrt{3(n_1^2 + n_2^2 + n_1 n_2)}$, where d is the inner tube diameter and a is the in-plane lattice parameter. Using $d = 3.1$ nm we obtain $n \approx 20$ for zigzag and $n_1 = n_2 \approx 13$ for armchair nanotubes. Tight-binding calculations by Rubio *et al.*⁷ show that the band gap in BN nanotubes decreases by 5% when the diameter of the BN sheets was lowered, both in zigzag and armchair nanotubes, from $d \sim \infty$ down to $d \approx 2$ nm for zigzag and $d \approx 3.6$ nm for armchair nanotubes, which corresponds to a chirality index of $n < 15$ respectively. Rubio *et al.*⁷ suggested that the formation of some sp^3 hybridization as due to the curvature of the sheets causes a reduction of the ionicity of the bonding and a reduction of the band gap. More recently, Okada *et al.*¹⁵ theoretically reported a reduction of the band gap by 10% in double wall BN nanotubes of zigzag chirality (9, 0) with respect to *h*-BN using the local-density approximation (LDA). They also interpreted that the appearance of some sp^3 hybridization due to the curvature of the BN sheets induces a different downward shift of the π and π^* orbitals leading to a decrease of the band gap as the tube diameter decreases. Owing to the fact that we are measuring multiwall tubes of likely mixed chirality and that the theoretical calculations consider single or double walled structures, the correlation between band-gap reduction and the averaged diameter observed in our samples seems to be in reasonable agreement with the gap reduction predicted by Rubio *et al.*⁷ and Okada *et al.*¹⁵ A decrease of the energy of the π - π^* transitions has also been reported for concentric shell fullerenes,³⁸ or more recently for single wall carbon nanotubes SWCNT's,³⁹ as compared to the value observed for graphite. In the case of the SWCNT's, the energy of the π - π^* transitions is found to decrease from 3.14 eV for graphite down to 2.95 eV for SWCNT's, (i.e., 6%). An alternative explanation of the downward shift of the transition ω_1 may arise from the enlargement of the BN unit cell, as observed by electron diffraction, and hence from a reduction of the number of effective electrons per volume unit n_{eff} contributing to the screening of the e - h interaction. Although the position of the $\sigma + \pi$ plasmon in *h*-BN is strongly dependent upon the sample texture and the direction of the momentum transfer, the interpretation above could be consistent with the observed reduction of the energy of this plasmon, i.e., from 25.5 eV for *h*-BN (Ref. 20) or 26.4 eV (pyrolytic *h*-BN,³³ $q \perp c$) down to 23.2 eV in the case of our BN nanotubes. Nevertheless, we have to note that, given the geometry of the nanotubes, the loss spectra measured here represent an average along the two principal crystal directions (a,b) and c so

that the exact position of the $\sigma + \pi$ plasmon along the nanotube axis (a,b) is unknown due to the appearance of the $\sigma + \pi$ plasmon along the c axis [23 eV in pyrolytic *h*-BN (Ref. 33)].

Band structure calculations^{26,30} of *h*-BN predict a momentum dispersion for the electronic excitations between π -derived bands along the L - M axis of the Brillouin zone, which is in agreement with what we observe in our measurements. This result signals that the degree of delocalization of the electronic excitations along the BN nanotubes is due to the fact that they are dominated by the band structure of the BN sheets, which is also supported by the similar momentum dispersion of the π plasmon of *h*-BN as reported by Tarrío *et al.*³³ However, a matter of discrepancy is observed when comparing the degree of q dispersion of the $\sigma + \pi$ plasmon of our BN nanotubes and the *h*-BN, which is larger in the case of the BN nanotubes. Considering the similarities between lattice structure and chemical nature of both materials one would expect the same overall behavior of both π and $\sigma + \pi$ plasmons upon q , as it was observed in other compounds like SWCNT's (Ref. 38) or concentric shell fullerenes³⁸ with respect to graphite. Further q -dependent EELS studies of pyrolytic and polycrystalline *h*-BN may be carried out in order to clarify these discrepancies.

The double peak feature located at 11 and 12 eV in the loss function (cf. Fig. 3) and in ε_2 stems from interband transitions of σ - π character, in agreement to band-structure calculations of *h*-BN reported by Xu *et al.*³⁰ and with q -orientation-dependent measurements³³ of the loss function in *h*-BN single crystals. ε_2 calculated by Xu *et al.*³⁰ for different q orientations in *h*-BN ($q \perp$ and $q \parallel$ to the c axis) shows a good agreement in energy and shape with our results in the region around 11.5 eV indicating the similarities between the optical response of the multiwall BN nanotubes and *h*-BN. The energy, width, and strength of the excitation ω_5 (σ - σ^* transitions) are also well reproduced in the calculations by Xu *et al.*³⁰ and these are in good agreement with that reported by Terauchi *et al.*²⁰ in multiwall BN nanotubes.

V. CONCLUSIONS

In summary, we have presented electronic structure studies of multiwall BN nanotubes as obtained by a substitution reaction from SWCNT templates. TEM images and B1s and N1s excitation edges of the grown material reveal the presence of multiwall BN nanotubes with an inner diameter of 3.1 nm and with a larger interplanar distance than in *h*-BN. The electronic properties of the multiwall BN nanotubes as derived from the q -dependent dielectric function $\varepsilon(\omega, q)$ are dominated by the band structure of the hexagonal-like BN sheets, as revealed by the large degree of momentum dispersion observed for the π and $\sigma + \pi$ plasmons, in agreement with that previously reported for different graphitic allotropic forms. The electronic σ - σ (ω_5) and σ - π ($\omega_{3,4}$) transitions resemble very good the theoretical and experimental data reported in the literature for *h*-BN, also confirming the similarities between the band structures of BN nanotubes and *h*-BN.

We have observed an energy reduction of the lowest energy feature in the loss function of the BN nanotubes with respect to that reported for bulk *h*-BN most likely due to the decrease of the band gap caused by the curvature of the

sheets and the appearance of some sp^3 hybridization. The decrease of n_{eff} as due to the reduction of the volume of the unit cell can also contribute to the downward shift of this feature. The observed reduction of the band gap agrees reasonably well with band-structure calculations of BN nanotubes.

ACKNOWLEDGMENTS

This work is funded by the network SATURN. The technical support from K. Müller and R. Hübel is also appreciated. One of the authors, G.G.F., acknowledges the financial support of the European Community.

-
- *Author to whom correspondence should be addressed. Fax: +49 351 4659 440; email address: g.fuentes@ifw-dresden.de
- ¹S. Ijima, *Nature* (London) **354**, 56 (1991).
 - ²J. W. G. Wildöer, L. C. Venema, A. G. Rinzler, R. E. Smalley, and C. Dekker, *Nature* (London) **391**, 59 (1998).
 - ³O. M. Küttel, O. Groening, C. Emmenegger, and L. Schlapbach, *Appl. Phys. Lett.* **73**, 2113 (1998).
 - ⁴Y. Xue and S. Datta, *Phys. Rev. Lett.* **23**, 4844 (1999).
 - ⁵F. Okuyama, T. Hayashi, and Y. Fujimoto, *J. Appl. Phys.* **84**, 1626 (1998).
 - ⁶C. Prados, P. Crespo, J. M. González, A. Hernando, J. F. Marco, R. Gancedo, N. Grobert, M. Terrones, R. W. Walton, and H. W. Kroto, *Phys. Rev. B* **65**, 113405 (2002).
 - ⁷A. Rubio, J. L. Corkill, and M. Cohen, *Phys. Rev. B* **49**, 5081 (1994).
 - ⁸X. D. Bai, E. G. Wang, and J. Yu, *Appl. Phys. Lett.* **77**, 67 (2000).
 - ⁹A. Loiseau, F. Willaime, N. Demoncey, G. Hug, and H. Pascal, *Phys. Rev. Lett.* **76**, 4737 (1996).
 - ¹⁰W. Han, Y. Bando, K. Kurashima, and T. Sato, *Appl. Phys. Lett.* **73**, 3085 (1998).
 - ¹¹D. Golberg, Y. Bando, W. Han, K. Kurashima, and T. Sato, *Chem. Phys. Lett.* **308**, 337 (1999).
 - ¹²D. Golberg, Y. Band, K. Kurashima, and T. Sato, *Chem. Phys. Lett.* **323**, 185 (2000).
 - ¹³C. Y. Zhi, J. D. Guo, X. D. Bai, and E. G. Wang, *J. Appl. Phys.* **91**, 5325 (2002).
 - ¹⁴X. Blase, A. Rubio, S. G. Louie, and M. Cohen, *Europhys. Lett.* **28**, 335 (1994).
 - ¹⁵S. Okada, S. Saito, and A. Oshiyama, *Phys. Rev. B* **65**, 165410 (2002).
 - ¹⁶X. Blase, A. Rubio, S. G. Louie, and M. Cohen, *Phys. Rev. B* **51**, 6868 (1995).
 - ¹⁷Y. H. Kim, K. J. Chang, and S. G. Louie, *Phys. Rev. B* **63**, 205408 (2001).
 - ¹⁸E. Hernández, C. Goze, P. Bernier, and A. Rubio, *Phys. Rev. Lett.* **80**, 4502 (1998).
 - ¹⁹S. Okada, S. Saito, and A. Oshiyama, *Phys. Rev. B* **64**, 201303 (2001).
 - ²⁰M. Terauchi, M. Tanaka, T. Matsumoto, and Y. Saito, *J. Electron Microsc. J.* **47**, 319 (1998).
 - ²¹O. Jost, A. A. Gorbunov, J. Möller, W. Pompe, A. Graff, R. Friedlein, X. Liu, M. S. Golden, and J. Fink, *Chem. Phys. Lett.* **339**, 297 (2001).
 - ²²J. Fink, *Adv. Electron. Electron Phys.* **75**, 121 (1989), and references therein.
 - ²³Y. Saito, T. Yoshikawa, S. Bandow, M. Tomita, and T. Hayashi, *Phys. Rev. B* **48**, 1907 (1993).
 - ²⁴Z. G. Li, P. J. Fargan, and L. Liang, *Chem. Phys. Lett.* **207**, 148 (1993).
 - ²⁵R. Gago, I. Jiménez, J. M. Albella, and L. J. Terminello, *Appl. Phys. Lett.* **78**, 3430 (2001).
 - ²⁶John Robertson, *Phys. Rev. B* **29**, 2131 (1984).
 - ²⁷I. Jiménez, A. Jankowski, L. J. Terminello, J. A. Carlisle, D. G. J. Sutherland, G. L. Doll, J. V. Mantese, W. M. Tong, D. K. Shuh, and F. J. Himpsel, *Appl. Phys. Lett.* **68**, 2816 (1996).
 - ²⁸I. Tanaka and H. Araki, *Phys. Rev. B* **60**, 4944 (1999).
 - ²⁹M. Knupfer, J. Fink, E. Zojer, G. Leising, and D. Fichou, *Chem. Phys. Lett.* **318**, 585 (2000).
 - ³⁰Y.-N. Xu and W. Y. Ching, *Phys. Rev. B* **44**, 7787 (1991).
 - ³¹R. Greick, C. H. Perry, and G. Rupprecht, *Phys. Rev.* **146**, 543 (1966).
 - ³²R. Resta, *Phys. Rev. B* **16**, 2717 (1977).
 - ³³C. Tarrío and S. E. Schnatterly, *Phys. Rev. B* **40**, 7852 (1989).
 - ³⁴K. Zeppenfeld, *Z. Phys.* **243**, 229 (1971).
 - ³⁵T. Pichler, M. Knupfer, M. S. Golden, J. Fink, A. Rinzler, and R. E. Smalley, *Phys. Rev. Lett.* **80**, 4729 (1998).
 - ³⁶X. Liu, T. Pichler, M. Knupfer, M. S. Golden, J. Fink, D. A. Walters, M. J. Casavant, J. Schmidt, and R. E. Smalley, *Synth. Met.* **121**, 1183 (2001).
 - ³⁷X. Liu, T. Pichler, M. Knupfer, M. S. Golden, J. Fink, H. Kataura, Y. Achiba, K. Hirahara, and S. Ijima, *Phys. Rev. B* **65**, 045419 (2002).
 - ³⁸T. Pichler, M. Knupfer, M. S. Golden, J. Fink, and T. Cabioch, *Phys. Rev. B* **63**, 155415 (2001).
 - ³⁹X. Liu, T. Pichler, M. Knupfer, M. S. Golden, J. Fink, H. Kataura, and Y. Achiba, *Phys. Rev. B* **66**, 045411 (2002).